

Entropy-Driven Liquid Electrolytes for Lithium Batteries

Wang, Qidi; Zhao, Chenglong; Yao, Zhenpeng; Wang, Jianlin; Wu, Fangting; Kumar, Sai Govind Hari; Ganapathy, Swapna; Eustace, Stephen; Wagemaker, Marnix

DOI

[10.1002/adma.202210677](https://doi.org/10.1002/adma.202210677)

Publication date

2023

Document Version

Final published version

Published in

Advanced Materials

Citation (APA)

Wang, Q., Zhao, C., Yao, Z., Wang, J., Wu, F., Kumar, S. G. H., Ganapathy, S., Eustace, S., & Wagemaker, M. (2023). Entropy-Driven Liquid Electrolytes for Lithium Batteries. *Advanced Materials*, 35(17). <https://doi.org/10.1002/adma.202210677>

Important note

To cite this publication, please use the final published version (if applicable).
Please check the document version above.

Copyright

Other than for strictly personal use, it is not permitted to download, forward or distribute the text or part of it, without the consent of the author(s) and/or copyright holder(s), unless the work is under an open content license such as Creative Commons.

Takedown policy

Please contact us and provide details if you believe this document breaches copyrights.
We will remove access to the work immediately and investigate your claim.

Entropy-Driven Liquid Electrolytes for Lithium Batteries

Qidi Wang, Chenglong Zhao,* Zhenpeng Yao, Jianlin Wang, Fangting Wu, Sai Govind Hari Kumar, Swapna Ganapathy, Stephen Eustace, Xuedong Bai, Baohua Li, Jun Lu, and Marnix Wagemaker*

Developing liquid electrolytes with higher kinetics and enhanced interphase stability is one of the key challenges for lithium batteries. However, the poor solubility of lithium salts in solvents sets constraints that compromises the electrolyte properties. Here, it is shown that introducing multiple salts to form a high-entropy solution, alters the solvation structure, which can be used to raise the solubility of specific salts and stabilize electrode–electrolyte interphases. The prepared high-entropy electrolytes significantly enhance the cycling and rate performance of lithium batteries. For lithium-metal anodes the reversibility exceeds 99%, which extends the cycle life of batteries even under aggressive cycling conditions. For commercial batteries, combining a graphite anode with a $\text{LiNi}_{0.8}\text{Co}_{0.1}\text{Mn}_{0.1}\text{O}_2$ cathode, more than 1000 charge–discharge cycles are achieved while maintaining a capacity retention of more than 90%. These performance improvements with respect to regular electrolytes are rationalized by the unique features of the solvation structure in high-entropy electrolytes. The weaker solvation interaction induced by the higher disorder results in improved lithium-ion kinetics, and the altered solvation composition leads to stabilized interphases. Finally, the high-entropy, induced by the presence of multiple salts, enables a decrease in melting temperature of the electrolytes and thus enables lower battery operation temperatures without changing the solvents.

1. Introduction

Synthesizing new materials through increasing their configurational entropy is an emerging concept in materials science. High-entropy (HE) alloys,^[1,2] typically consisting of five or more principal elements, facilitate the formation of solid-solution phases with simple structures.^[3] This has been extended to entropy-stabilized functional oxides and fluorites and other solid chemistries.^[4,5] For a given system, the configurational entropy will increase with the number of principle components introduced, which will lower the Gibbs free energy, manifesting itself in extended solubility limits through the entropy-driven structural stabilization.^[6] Thereby, increasing the entropy to stabilize phases provides opportunities to design functional materials for various fields, including catalysis,^[7] dielectrics,^[8] and energy storage,^[9] making it possible to resolve challenging issues in traditional systems.

Q. Wang, C. Zhao, S. Ganapathy, M. Wagemaker
Department of Radiation Science and Technology
Delft University of Technology
Delft 2629JB, The Netherlands
E-mail: c.zhao-1@tudelft.nl; m.wagemaker@tudelft.nl

Z. Yao
The State Key Laboratory of Metal Matrix Composites
School of Materials Science and Engineering
Center of Hydrogen Science
Shanghai Jiao Tong University
Shanghai 200240, China

J. Wang, X. Bai
State Key Laboratory for Surface Physics
Institute of Physics
Chinese Academy of Sciences
Beijing 100190, China

 The ORCID identification number(s) for the author(s) of this article can be found under <https://doi.org/10.1002/adma.202210677>.

© 2023 The Authors. Advanced Materials published by Wiley-VCH GmbH. This is an open access article under the terms of the Creative Commons Attribution-NonCommercial-NoDerivs License, which permits use and distribution in any medium, provided the original work is properly cited, the use is non-commercial and no modifications or adaptations are made.

DOI: 10.1002/adma.202210677

F. Wu, B. Li
Shenzhen Key Laboratory on Power Battery Safety
and Shenzhen Geim Graphene Center
School of Shenzhen International Graduate
Tsinghua University
Guangdong 518055, China

S. G. H. Kumar
Department of Chemistry and Computer Science
University of Toronto
Ontario M5S 3H6, Canada

S. Eustace
Department of Biotechnology
Delft University of Technology
Delft 2629HZ, The Netherlands

J. Lu
College of Chemical and Biological Engineering
Zhejiang University
Hangzhou 310027, China

Compared to solids, liquids naturally exhibit a larger entropy because of their more dynamic and disordered nature. Dissolving solutes in solvents to form a uniform solution is thermodynamically similar to the formation of single-phase solid compounds. Solute and solvents exhibit different compatibilities, as expressed by their free energy of solvation (mixing) (ΔG_{mix}), which is built up by the enthalpy of mixing (ΔH_{mix}) and the entropy of mixing (ΔS_{mix}) through the combination of the 1st and 2nd laws of thermodynamics

$$\Delta G_{\text{mix}} = \Delta H_{\text{mix}} - T\Delta S_{\text{mix}} \quad (1)$$

ΔS_{mix} can be expressed in terms of the composition as follows

$$\Delta S_{\text{mix}} = -nR \sum_i x_i \ln x_i \quad (2)$$

where R is the gas constant, n the total number of moles and x_i the mole fraction of component i . In a conventional electrolyte with few components, the solubility of the solutes is determined by the competition between ΔH_{mix} (a more positive value leads to a lower solubility) and ΔS_{mix} (a larger value increases the solubility). When the solubility limit is exceeded at specific conditions (i.e., temperature and pressure), the solute will precipitate, forming a heterogeneous system, which is conceptually similar to spinodal decomposition in solids (Figure 1a). Therefore, introducing multiple components to increase the entropy of mixing (ΔS_{mix}), in principle, represents a strategy to promote the formation of homogeneous solutions of liquids (Figure 1b), which can be relevant for a wide number of applications.

This is especially relevant for batteries (e.g., lithium-ion batteries), where adding salt and solvent additives in liquid electrolytes plays a crucial role in achieving a long cycle life, through

the formation of stable interphases, and improving lithium-ion transport to lower the internal resistance.^[10–13] However, one of the main challenges is the compatibility of salts and solvents to form uniform solutions, which imposes restrictions in developing high-performance electrolytes. An exponent of this is LiNO_3 , a widely used additive in ether-based electrolytes to increase the interphase stability with electrodes.^[14] However, it is considered to be incompatible with commercial high-voltage carbonate solvents,^[15,16] such as ethylene carbonate (EC)/dimethyl carbonate (DMC) (Note S1, Supporting Information). Therefore, increasing the LiNO_3 solubility in carbonates through other routes has attracted wide attention. Introducing Lewis acid salts^[17,18] or cosolvents^[19,20] has recently been reported to weaken the Coulombic interaction between NO_3^- and Li^+ and thus improve its solubility. However, the corresponding concerns is that these extra additives compromise the electrolyte properties and degrade the interphase stability due to their intrinsic reactivity during (dis)charge.^[19–23] Therefore, new strategies to improve the solubility of specific salts, especially in commercially viable electrolytes (e.g., EC/DMC) are desirable.

Here, we show that introducing multiple, commonly used lithium salts in commercial carbonate solvents enhances the solubility of specific salts by raising the entropy of mixing, using LiNO_3 as a proof of concept. The resulting high entropy (HE) liquid electrolytes are shown to have a much more diverse solvation structure, where more salt anion groups interact with the lithium ions. A consequence of the higher disorder weakens the interaction between lithium ions with both salts and solvents. This results in the formation of uniform liquid electrolytes, that can achieve more stable electrode/electrolyte interphases and higher lithium-ion mobility, responsible for

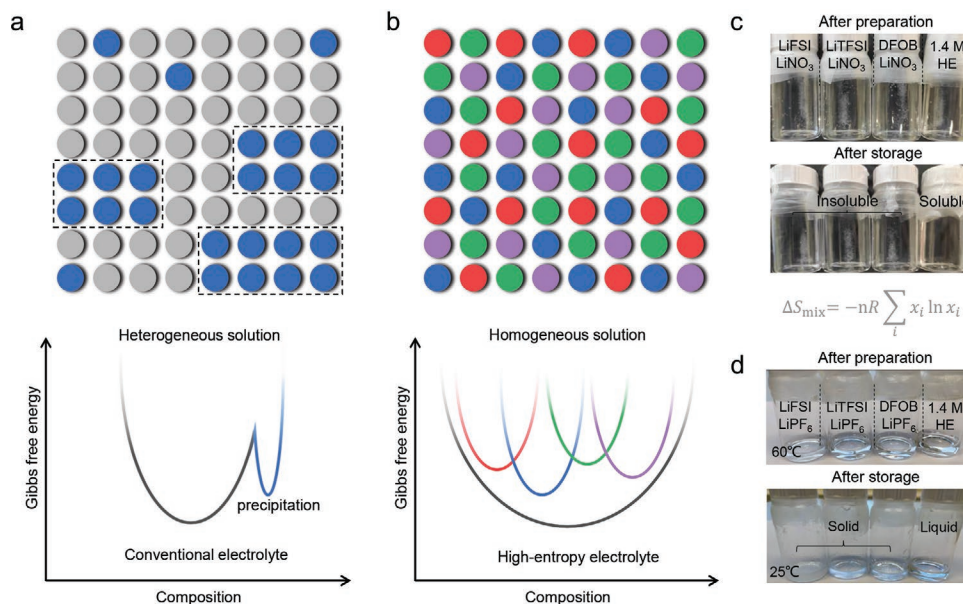


Figure 1. Improving the stability of liquid electrolytes through increasing entropy of mixing. a) Schematic diagram of compositional structure and energy in heterogeneous solution with precipitation of a component due to a limited solubility. b) Schematic diagram of compositional structure and energy in a homogeneous solution by mixing more components to increase the entropy of mixing. c) Solubility of different salts in EC/DMC (1:1 by weight) with 5% FEC: from left to right 0.1 M LiFSI/0.1 M LiNO_3 /1.0 M LiPF_6 , 0.1 M LiTFSI/0.1 M LiNO_3 /1.0 M LiPF_6 , 0.1 M LiDFOB/0.1 M LiNO_3 /1.0 M LiPF_6 , and 0.1 M LiFSI/0.1 M LiTFSI/0.1 M LiDFOB/0.1 M LiNO_3 /1.0 M LiPF_6 (1.4 M HE). The white precipitation in the electrolytes is LiNO_3 -related compounds. d) Liquid to solid phase transition behavior of different salts in the EC solvent: from left to right 0.4 M LiFSI/1.0 M LiPF_6 , 0.4 M LiTFSI/1.0 M LiPF_6 , 0.4 M LiDFOB/1.0 M LiPF_6 , 1.4 M HE. The EC-based electrolytes are prepared at around 60 °C and stored at room temperature.

substantial improvements in lithium battery performances. It should be noted this is essentially different from the mixing of several solvents with 1 up to 3 salts, also referred to “HE electrolytes,” where the functional properties of entropy stabilization on the system are not considered.^[24]

2. Formation and Solvation Structures of the Entropy-Driven Electrolyte

The commercial 1.0 M LiPF₆ in EC/DMC carbonate electrolyte (1:1 by weight) with 5% fluoroethylene carbonate (FEC) is selected as baseline electrolyte, which has negligible solubility for LiNO₃ (≤1000 ppm).^[15,16] The commercially available salts LiFSI, LiTFSI, and LiDFOB are introduced based on their relative innocuousness and good solubility in carbonates, and combined to raise the entropy of the electrolyte. The presence of these multiple salt components increases the solubility of LiNO₃ up to 0.1 M (Figure S1, Supporting Information), leading to the obtained HE electrolyte composition of 0.1 M LiFSI/0.1 M LiTFSI/0.1 M LiDFOB/0.1 M LiNO₃/1.0 M LiPF₆ in EC/DMC (1:1 by weight) with 5% FEC, henceforth referred to as 1.4 M HE-EDF. To investigate the influence of the individual salts on promoting LiNO₃ dissolution, electrolytes were prepared with each salt, all combined with 0.1 M LiNO₃ into 1.0 M LiPF₆ in EC/DMC with 5% FEC (Figure 1c). None of the individual salt is able to promote LiNO₃ dissolution as demonstrated in Figure 1c where insoluble LiNO₃ is clearly observed, and thus the combination of multiple salts is held responsible for the increased LiNO₃ solubility. The same strategy is further examined in an ether-based system (Figure S2 and Note S2, Supporting Information), also resulting in a significant improvement of the LiNO₃ solubility by raising the entropy of mixing through introducing multiple salts. In the HE electrolyte, the larger variety of solvation interactions are anticipated to be responsible for the larger entropy of mixing, thereby decreasing the Gibbs Free energy and thus increasing the solubility. In addition, this can be expected to influence the temperature-dependent properties of the electrolytes due to its diverse solvation structure. To demonstrate this, the pure EC solvent that is solid at room temperature (melting point ≈36.4 °C), is mixed with each single salt as well as with the combination of multiple salts to form a HE system. After preparation at 60 °C, all electrolytes are clear, representing uniform solutions. However, during cooling to room temperature, the electrolytes with the single extra salt turn into semisolid or solid, except for the HE electrolyte, which maintains liquid for a longer period of several hours (Figure 1d). This suggests that raising the entropy can also be an effective strategy to improve the electrolyte properties for lower temperature applications as was also suggested for introducing specific solvents, in which case the melting point of the solvents can be expected to play a dominant role.^[24,25]

The very small solubility of LiNO₃ in 1.0 M LiPF₆-EDF (≤1000 ppm)^[15,16] increases several orders of magnitude in the HE electrolyte (Figure S3, Supporting Information), suggesting that the solvation structure in the HE electrolyte is very different compared to that in the single salt electrolytes. Raman spectroscopy demonstrates that the 1.4 M HE-EDF electrolyte has a weaker solvation interaction between the lithium-ions and EDF solvents, as compared to the single-salt 1.4 M LiPF₆-

EDF electrolyte and the other control electrolytes, reflected by the weaker coordinated peak (Figure 2a; Figures S4 and S5 and Note S3, Supporting Information). Consistently, a downfield shift in the ⁷Li NMR spectra is observed for the 1.4 M HE-EDF electrolyte (Figure 2b; Figure S6 and Note S4, Supporting Information) indicating weaker interactions of lithium ions with both solvents and anion groups. This can be attributed to the HE composition, which effectively increases the disorder of the system, presenting a conceptually different mechanism compared to the reported increase in the LiNO₃ solubility,^[17–20,26] and in high-salt concentration electrolytes.^[27] In general, the decreased solvation interaction of lithium ions with solvents will result in the relatively increased interaction with anion groups from salts and vice versa, however, the average solvation strength is found to decrease, improving the lithium-ion transport.^[17–20,26,27] Therefore, benefiting from the altered solvation structure and interactions, a higher conductivity and lower viscosity of (1.76 vs 2.62 mPa s) is achieved in the 1.4 M HE-EDF compared with the control electrolytes (the inset of Figure 2b).

Molecular dynamics (MD) simulations indicate that the various anion species in 1.4 M HE-EDF electrolyte result in a rich diversity of over 100 types of lithium-ion solvation environments, much more than what is obtained from the 1.4 M LiPF₆-EDF electrolyte (Figures S7–S11 and Tables S1 and S2, Supporting Information). Based on the radial distribution function (RDF), the Li–F interaction, between PF₆[−] and lithium ions, is decreased in the 1.4 M HE-EDF electrolyte as compared to the 1.4 M LiPF₆-EDF electrolyte. In contrast the Li–O, Li–N, Li–S interactions from the various anion groups are enhanced, which is anticipated to promote the formation of an anion-dominated and inorganic-rich SEI composition that will increase the interphase stability as will be discussed below (Figure S12, Supporting Information). The simulated self-diffusion coefficient of the 1.4 M HE-EDF electrolyte (1.9 × 10^{−6} cm² s^{−1}) is larger than that of the 1.4 M LiPF₆-EDF electrolyte (1.2 × 10^{−6} cm² s^{−1}) (Figure S13, Supporting Information), in agreement with the measured improvement in the conductivity. The higher lithium-ion mobility in the 1.4 M HE-EDF electrolyte is also confirmed by the larger lithium transference number (Figure S14, Supporting Information) and higher exchange current density (Figure S15, Supporting Information). This entropy induced improved ion transport can be explained by excess entropy scaling in liquid systems,^[28,29] where the increasing number of components leads to a wider distribution in diffusional barriers from the diverse solvation structures, enhancing diffusional channels via the available percolation network.^[30] In addition, the 1.4 M HE-EDF electrolyte has a slightly higher reduction potential for the decomposition of salts at around 1.23 V (Figure S16, Supporting Information). After the initial cycles, the reduction peak intensity decreases in the 1.4 M HE-EDF electrolyte and stabilizes during subsequent cycles, indicating that a stable SEI has formed during the initial cycle.^[31]

3. Anode Interphase Stability

The compatibility with lithium-metal anodes is evaluated by Coulombic efficiency (CE) measurements.^[32,33] The 1.4 M HE-EDF electrolyte shows a higher average CE, exceeding 99%, and a lower overpotential compared to the single-salt 1.4 M

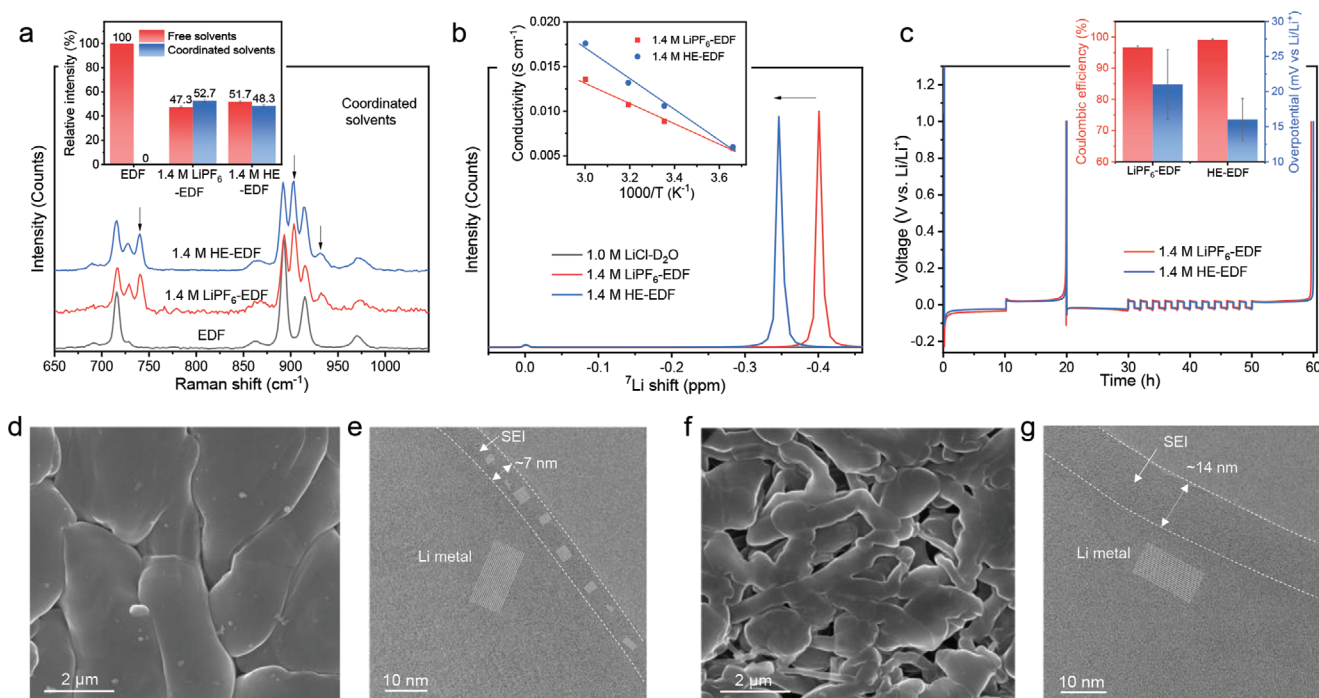


Figure 2. Solvation structure and compatibility of the HE electrolyte with the lithium-metal anode. a) Raman spectra of the EDF solvent, 1.4 M LiPF₆-EDF, and 1.4 M HE-EDF. The black arrows mark the peaks that represent lithium ions coordinated to solvents. The insert shows the distribution of free solvent and coordinated solvent (Li⁺-EDF) from the peak fitting results (Figure S5, Supporting Information). b) Liquid ⁷Li NMR spectra of 1.4 M LiPF₆-EDF and 1.4 M HE-EDF electrolytes. The inset shows the lithium ionic conductivity of the 1.4 M LiPF₆-EDF and 1.4 M HE-EDF electrolytes at various temperatures. c) Lithium-metal Coulombic efficiency (CE) in Li||Cu cells using different electrolytes. d,f) SEM images of deposited lithium metal on Cu foil at a current density of 0.5 mA cm⁻² to 1 mAh cm⁻² in 1.4 M HE-EDF electrolyte (d) and 1.4 M LiPF₆-EDF electrolyte (f). e,g) Cryo-transmission electron microscopy (Cryo-TEM) images showing microstructure of deposited lithium metal and interphase with 1.4 M HE-EDF electrolyte (e) and 1.4 M LiPF₆-EDF electrolyte (g).

LiPF₆-EDF electrolyte (Figure 2c), further confirmed by the galvanostatic cycling of Li||Cu and Li||Li cells (Figures S17–S19, Supporting Information). To determine the origin of the improved performance of the 1.4 M HE-EDF electrolyte in combination with a lithium-metal anode, the plating/stripping morphology of lithium metal is investigated using scanning electron microscopy (SEM). The deposited lithium metal in the 1.4 M HE-EDF electrolyte is compact and well connected to the Cu substrate with particle sizes around several micrometers (Figure 2d; Figures S20 and S21, Supporting Information). In contrast, the 1.4 M LiPF₆-EDF electrolyte results in porous and whisker-like dendritic lithium deposits that are less-well connected to the Cu (Figure 2f; Figure S21, Supporting Information). After stripping, a porous morphology with some residual dendritic lithium is observed for 1.4 M LiPF₆-EDF electrolyte (Figure S22, Supporting Information) whereas much less residual lithium metal is left behind for 1.4 M HE-EDF electrolyte, indicating more complete and homogenous stripping (Figures S22 and S23, Supporting Information). The denser and better-connected lithium-metal deposits formed in the 1.4 M HE-EDF electrolyte are beneficial for electron transport, allowing efficient stripping and suppressing the formation of inactive lithium.^[31] At the same time, the compact deposits minimize the exposed surface area resulting in less electrolyte decomposition, which in turn suppresses the formation of porous lithium on subsequent cycling. To further investigate the lithium-metal morphology and SEI properties, cryogenic transmission electron microscopy (cryo-TEM) is conducted at -170 °C.^[34] In the 1.4 M HE-EDF electrolyte,

large lithium-metal deposits are observed, but with a thin SEI layer (Figure 2e; Figure S24, Supporting Information). In sharp contrast, the 1.4 M LiPF₆-EDF electrolyte shows whisker and needle-like deposits (Figures S25 and S26, Supporting Information) and a thicker SEI (Figure 2g). The SEI composition and structures are also different, being inorganic dominated for the 1.4 M HE-EDF electrolyte (Figure 2e; Figure S24, Supporting Information), implying that more anion groups participate in the SEI formation.^[35] Whereas, for the 1.4 M LiPF₆-EDF electrolyte a carbon-rich amorphous structure is observed, driven by decomposition of the solvents (Figure S26, Supporting Information). The SEI composition is further studied using X-ray photoelectron spectroscopy (XPS) (Figures S27–S35 and Note S5, Supporting Information), where O 1s, F 1s, and N 1s spectra confirm that the inorganic Li-F, Li-N, B-F, Li-O, and B-O species dominate the SEI in the 1.4 M HE-EDF electrolyte. The presence of these species suggests a more facile and homogeneous lithium-ion supply, supporting dense lithium-metal growth. This explains the better reversibility of the lithium-metal anode in 1.4 M HE-EDF compared with 1.4 M LiPF₆-EDF electrolyte. To study the lithium loss during cycling, operando solid-state ⁷Li NMR^[36,37] is conducted in anode-less Cu||LiFePO₄ cells (Note S6, Supporting Information). Upon charge, lithium deposition occurs on the Cu electrode and the lithium-metal resonance appears. At the end of discharge, the lithium-metal peak remains, indicating the formation of “dead” lithium (Figures S36 and S37, Supporting Information). In both electrolytes, the integrated intensity of the lithium-metal peak grows

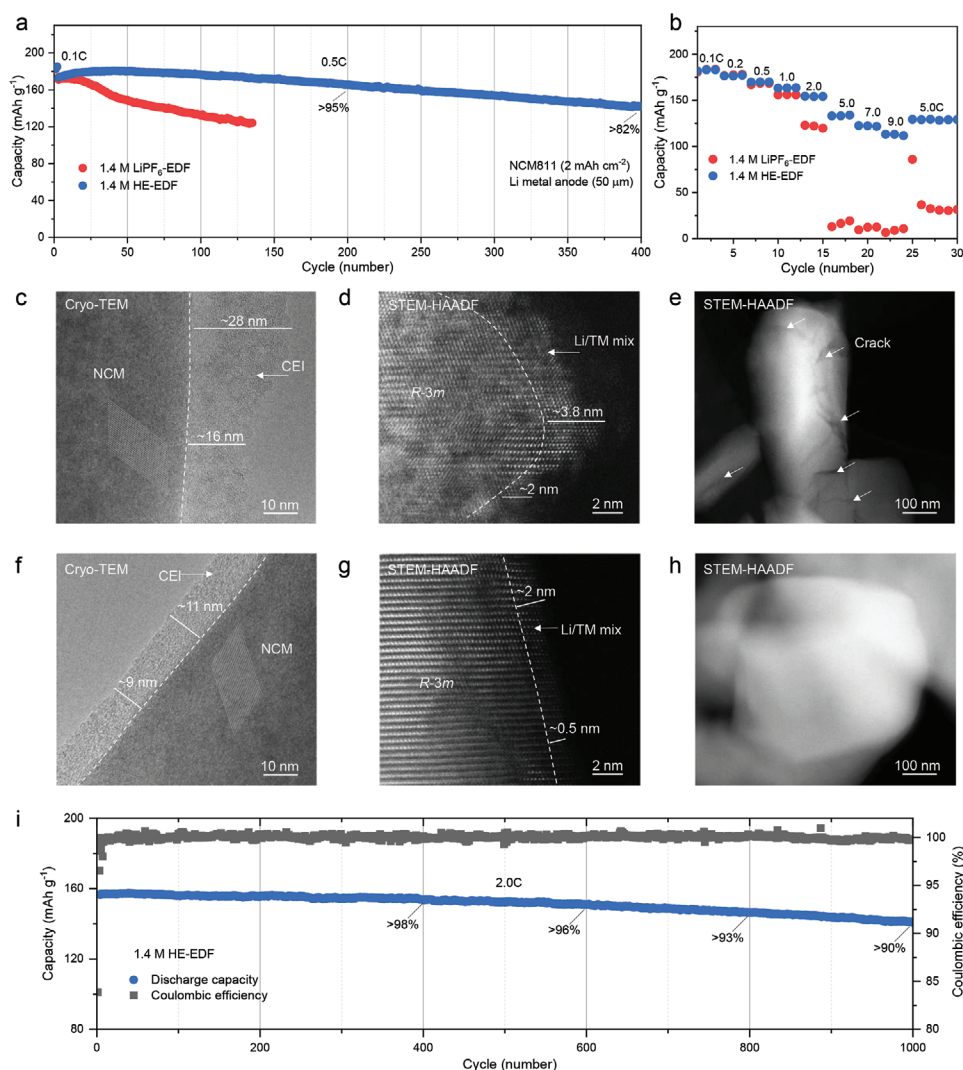


Figure 3. Electrochemical performance and cathode interphase stability of HE electrolyte. a) Capacity retention of Li||NCM811 cells with 1.4 M LiPF₆-EDF or 1.4 M HE-EDF electrolytes cycled between 2.8 and 4.3 V with 0.1C (1.0C = 180 mA g⁻¹) for three cycles and 0.5C for the following cycles. The areal capacity of NCM811 electrode is 2 mAh cm⁻² and the lithium-metal anode is 50 μm. b) Rate performance of Li||NCM811 cells cycled between 2.8 and 4.3 V under various current densities in different electrolytes. c, f) Cryo-TEM images of NCM811 cathode electrolyte interphase after cycling in 1.4 M LiPF₆-EDF (c) and 1.4 M HE-EDF (f) electrolytes. d, g) High resolution STEM-HAADF images of NCM811 cathode after cycling in 1.4 M LiPF₆-EDF (d), and 1.4 M HE-EDF (g) electrolytes. e, h) Low-magnification STEM-HAADF images of primary NCM811 particle morphology after cycling in 1.4 M LiPF₆-EDF (e) and 1.4 M HE-EDF (h) electrolytes. i) Capacity retention of graphite||NCM811 cells with the 1.4 M HE-EDF electrolyte cycled between 3.0 and 4.2 V at 0.1C rate for first three cycles and 2.0C for following cycles. The capacity ratio of the negative over the positive electrode is in the range of 1.05–1.10.

linearly during charging (Figure S38, Supporting Information), but less “dead” lithium is observed in the 1.4 M HE-EDF electrolyte after discharging, and the accumulated “dead” lithium during the following cycles is strongly reduced, which is consistent with the better cycling stability observed for the HE electrolyte.

4. Cathode Interphase Stability

The oxidation stability of 1.4 M HE-EDF is evaluated by linear sweep voltammetry (LSV) in a Li||Al/C cell (Figure S39, Supporting Information), where the voltage of initial decomposition is around 4.7 V versus Li/Li⁺, higher than that of the 1.4 M LiPF₆-EDF electrolyte, which is promising for application in nickel-rich

cathodes. Thus, the electrolytes are evaluated in combination with LiNi_{0.8}Co_{0.1}Mn_{0.1}O₂ (NCM811) cathodes into Li||NCM811 cells. The cells were cycled in the voltage range of 2.8–4.3 V versus Li/Li⁺ with an NCM811 areal capacity of 2.0 mAh cm⁻² and a thickness of lithium metal in 50 μm. During the initial cycles at 0.1C, the cells with the different electrolytes show a similar discharge capacity around 180 mAh g⁻¹ (Figures S40 and S41, Supporting Information), but the long-term cycling stability of 1.4 M HE-EDF electrolyte is significantly improved over the 1.4 M LiPF₆-EDF electrolyte, resulting in a capacity retention of over 82% after 400 cycles at 0.5C (Figure 3a). The influence of LiNO₃ was also investigated by comparison with the 1.3 M HE-EDF electrolyte without LiNO₃. Even though not as good as 1.4 M HE-EDF, the cell with the 1.3 M HE-EDF electrolyte

exhibits an improved cycling stability compared to the 1.4 M LiPF₆-EDF (Figures S42–S44, Supporting Information). When increasing the current rate to 9.0C (1620 mA g⁻¹), the cells using 1.4 M HE-EDF electrolyte achieve more than 60% capacity retention (Figure 3b), much higher than that of the cells using 1.4 M HE-EDF electrolyte (Figure S45, Supporting Information), in line with the improved Li-ion mobility discussed above and the smaller impedance originating from the more stable interphase (Figure S46, Supporting Information). After cycling, the morphology of the cathodes is investigated by SEM. The secondary cathode particles in the 1.4 M HE-EDF electrolyte are well preserved, while cracks and pulverization of the secondary particles are observed for the 1.4 M LiPF₆-EDF electrolyte (Figure S47, Supporting Information). Despite the presence of multiple salts, the 1.4 M HE-EDF electrolyte does not show aluminum foil corrosion, as demonstrated by a stable anodic current at a polarization potential of 4.2 V versus Li/Li⁺ for 20 h (Figure S48, Supporting Information).

The structure and chemical composition of the air-sensitive CEI layers are studied by cryo-TEM. Compared to the pristine materials (Figure S49, Supporting Information), an amorphous CEI layer is formed at the surface of the particles with a thickness from 16 to 28 nm in the 1.4 M LiPF₆-EDF electrolyte (Figure 3c), which is thicker than the 9–11 nm in the 1.4 M HE-EDF electrolyte (Figure 3f). Atomic-resolution high-angle annular dark-field (HAADF) scanning transmission electron microscopy (STEM) images collected at room temperature reveal a mixed Li/TM (TM: transition metal) layer at the surface of the cathode particles with a thickness from around 2–3.8 nm in 1.4 M LiPF₆-EDF electrolyte after cycling, along with lattice distortions (Figure 3d). However, for the 1.4 M HE-EDF electrolyte, the mixing layer is much thinner and the layered structure is well preserved (Figure 3g), indicating that microstructural degradation and side reactions are effectively suppressed. In addition, the low-magnification STEM-HAADF images show cracks formed on the primary cathode particles after cycling in the 1.4 M LiPF₆-EDF electrolyte (Figure 3e; Figure S50, Supporting Information), whereas no obvious cracks are observed in 1.4 M LiPF₆-EDF electrolyte (Figure 3h), indicating the improved structural stability of the cathodes. The CEI compositions are studied by electron energy loss spectroscopy (EELS) (Figures S51 and S52, Supporting Information), in which the CEI formed in 1.4 M HE-EDF electrolyte shows more O-, F-, and N-containing components, compared with that in 1.4 M LiPF₆-EDF electrolyte, which is confirmed with XPS depth profiling analysis (Figures S53–S57 and Note S7, Supporting Information). This compositional distribution demonstrates that the CEI in the 1.4 M HE-EDF electrolyte is more stable due to its inorganic-rich species. Further, graphite||NCM811 full cells using the 1.4 M HE-EDF electrolyte are also tested (Figure 3i; Figure S58, Supporting Information), resulting in ≈90% capacity retention after 1000 cycles at 2.0C cycling rate, demonstrating this HE electrolyte has excellent potential for the use in practical lithium-ion batteries.

5. Temperature-Dependent Properties

Crystallization (freezing) upon cooling of electrolytes presents a bottleneck for low-temperature application of lithium

batteries.^[38] When the temperature decreases below the melting point, a phase transition from liquid to solid will occur, which considerably lowers the conductivity of the remaining liquid phase and may even block electrode pores, temporarily isolating sections of the active material and thus causing capacity loss. Thermodynamically, the melting temperature of electrolytes is determined by the Gibbs free energy, and decreasing this by increasing the entropy of mixing (S_{mix}) (Figure 4a) can be a promising strategy to lower the freezing point of the electrolyte.^[39] Here, we show that introducing multiple salts to form the HE composition lowers the freezing point, improving the low-temperature electrolyte properties. In line with the observations for the pure EC solvent in Figure 1d, the freezing point of the 1.4 M HE-EDF electrolyte is lower compared to the 1.4 M LiPF₆-EDF electrolyte (Figure S59, Supporting Information). However, the nature of the solvents has a larger impact on the freezing point, which remains the limitation of EC/DMC solvents. Generally, introducing solvents having lower melting points is the established route to achieve low-temperature battery performance.^[24,25] To investigate if the present multicomponent salt strategy can lower the melting point of low-temperature solvents even further, a combination of propylene carbonate (PC) and diethyl carbonate (DEC) solvents is investigated.^[10,11] A HE electrolyte consisting of five components with equal molar fractions salt of 0.15 M LiPF₆/0.15 M LiFSI/0.15 M LiTFSI/0.15 M LiDFOB/0.15 M LiNO₃ in PC/DEC (1:1) with 5% FEC (referred to as 0.75 M HE-PDF) is prepared (see the Experimental Section), where 0.15 M LiNO₃ can be dissolved in this mixed solvent. For comparison, a single salt electrolyte with the same molarity and solvents of 0.75 M LiPF₆ in PC/DEC with 5% FEC (referred to as 0.75 M LiPF₆-PDF) is prepared. The solvation structure of the HE electrolyte is studied at different temperatures using variable-temperature (VT) ⁷Li NMR experiments (Figure 4b,c). As temperature decreases, the ⁷Li resonance of the 0.75 M HE-PDF shows a smaller shift compared to the 0.75 M LiPF₆-PDF electrolyte, which demonstrates that introducing multiple salts stabilizes the solution when the temperature changes. The downfield shift of 0.75 M HE-PDF compared to 0.75 M LiPF₆-PDF at each temperature indicates a weaker solvation strength for the HE electrolyte, that can be expected to promote the lithium-ion kinetics.

Indeed, the HE-PDF electrolyte shows a higher conductivity (Figure 4d) and lithium transference number (0.456 vs 0.401 of the HE-PDF and LiPF₆-PDF electrolytes, respectively) as well as a higher exchange current density, confirming the improved bulk kinetics and charge transfer upon increasing the entropy (Figures S60–S62, Supporting Information). These properties are held responsible for the improved electrochemical performance reflected by the lower overpotential and higher average CE at different temperatures (Figures S63 and S64, Supporting Information). When cycled at –40 °C, the CE maintains larger than 80%, outperforming the 0.75 M LiPF₆-PDF with a CE around 30% (Figure 4e; Figure S65, Supporting Information).

In addition, the 0.75 M HE-PDF electrolyte shows a higher oxidation stability (Figure S66, Supporting Information), which can be applied to high-voltage cathode. The Li||NCM811 cells employing the different electrolytes are first evaluated at room temperature, both delivering similar initial charge and discharge voltage profiles with a specific capacity of around

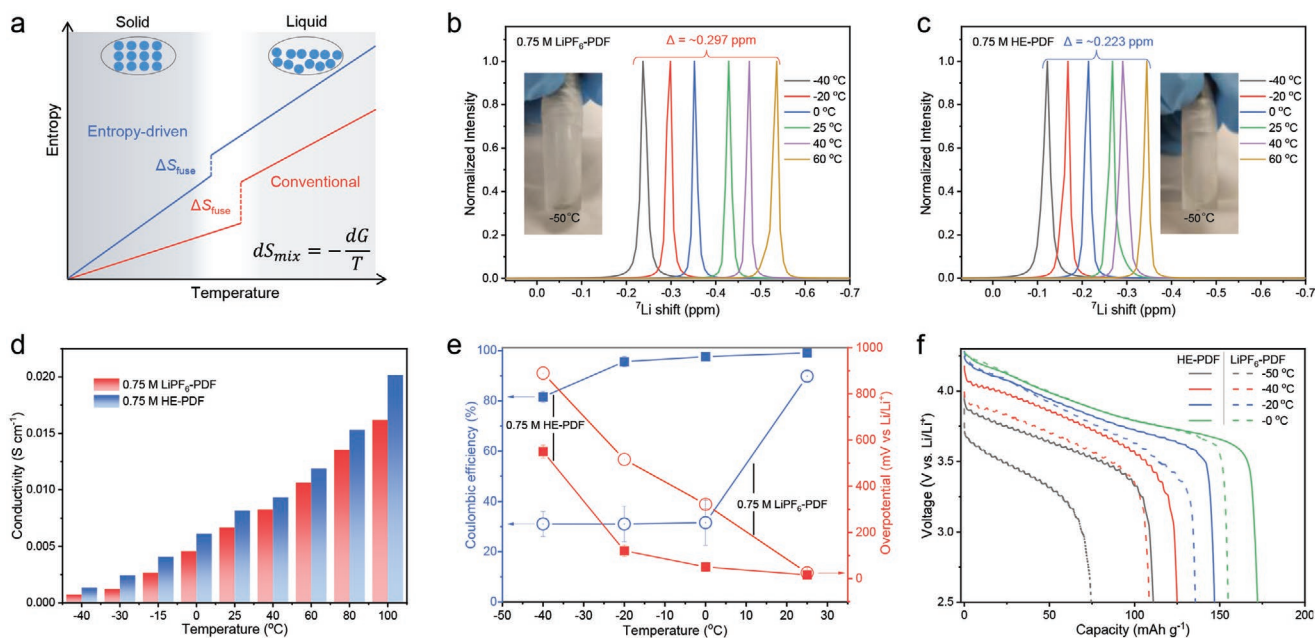


Figure 4. Temperature-dependent properties of HE electrolyte. a) Schematic diagram of the entropy evolution during phase changes as the function of temperature, where the blue line indicates the evolution trend of the HE electrolyte and the red line indicates the trend of a conventional electrolyte. b,c) Variable temperature liquid ^7Li NMR spectra of 0.75 M LiPF_6 in PC/DEC with 5% FEC (0.75 M LiPF_6 -PDF) (b) and 0.15 M LiPF_6 /0.15 M LiFSI /0.15 M LiTFSI /0.15 M LiDFOB /0.15 M LiNO_3 in PC/DEC with 5% FEC (0.75 M HE-PDF) (c). d) Ionic conductivity of the 0.75 M LiPF_6 -PDF and 0.75 M HE-PDF electrolytes at various temperatures. e) CE and overpotential of $\text{Li}||\text{Cu}$ cells at different temperatures with 0.75 M LiPF_6 -PDF or 0.75 M HE-PDF electrolyte. f) Discharge curves of $\text{Li}||\text{NCM811}$ cells cycling at 0.1C in 0.75 M LiPF_6 -PDF and 0.75 M HE-PDF electrolytes at different temperatures within the voltage range of 2.5–4.3 V at lower temperatures.

180 mAh g^{-1} (Figure S67, Supporting Information). Upon subsequent cycling, the cells with the 0.75 M HE-PDF electrolyte present much better cycling stability, retaining over 92% of its initial capacity after 300 cycles (Figure S68, Supporting Information). In comparison, the battery with the 0.75 M LiPF_6 -PDF electrolyte rapidly decays after 85 cycles. The battery performance is additionally evaluated at different temperatures (Figure 4f), where the 0.75 M HE-PDF electrolyte shows higher capacity retention at each temperature, also in these cases showing improved low-temperature performance compared to the 0.75 M LiPF_6 -PDF electrolyte. The low-temperature cycling stability of $\text{Li}||\text{NCM811}$ cells is measured at -20°C , where the cells with 0.75 M HE-PDF electrolyte exhibit the higher capacity retention of around 99% after cycles (Figures S69 and S70, Supporting Information). This is in line with the improved kinetics and enhanced interphase stability of this HE-PDF electrolytes as observed above.

6. Conclusion

The present work shows that increasing the entropy of mixing, by introducing multiple solutes, can be used to increase the stability of solvent–solute combinations, offering an attractive strategy to develop advanced electrolytes for (non)aqueous batteries such as lithium, sodium, zinc, magnesium, aluminum, and calcium batteries. The resulting electrolytes show improved lithium-ion kinetics and strongly altered solvation interactions due to the disordered solvation structure, a result of mixing several salts. This leads to the formation of more stable and

inorganic-rich interphases on the electrodes, strongly improving the electrochemical performance of batteries with practical applicability. Another aspect of the higher solvation-structure entropy is the lowering of the electrolyte melting point, thereby improving low-temperature performance.

This study using commercial carbonate electrolytes (i.e., LiPF_6 -EC/DMC) as starting point, should be considered a prototype study towards the general impact of increasing entropy induced by multiple salts, where strategies using advanced salts^[40] and/or solvents^[31] in combination with fluorine-rich^[41] or salt-concentrated^[27] can be expected to provide opportunities to further improve these electrolytes. Conceptually different to change the chemical and physical properties by introducing additional salts in electrolyte, the present work demonstrates that raising the entropy by adding multiple salts, induces a general and fundamental change in solvation interaction and structure, that (along with the specific salt chemistry) can be used to improve electrolyte properties. As liquids are widely utilized as reaction media in the synthesis of functional materials and drugs, introducing multiple components forming the HE solutions, can be considered an interesting route to alter the intermolecular interactions such that it can impact mass transfer processes relevant for preparation processes.

Supporting Information

Supporting Information is available from the Wiley Online Library or from the author.

Acknowledgements

Q.W., C.Z., Z.Y., and J.W. contributed equally to this work. The authors acknowledge the financial support by the Netherlands Organization for Scientific Research (NWO) grant 16122 (VICI). National Natural Science Foundation of China grant 51991344. Chinese Academy of Sciences grant XDB33000000. China Postdoctoral Science Foundation grant 2020M680541. Special Fund Project for Strategic Emerging Industry Development of Shenzhen grant 20170428145209110. Local Innovative and Research Teams Project of Guangdong Pearl River Talents Program grant 2017BT01N111.

Conflict of Interest

The authors declare no conflict of interest.

Data Availability Statement

The data that support the findings of this study are available from the corresponding author upon reasonable request.

Keywords

entropy-driven electrolytes, high-entropy electrolytes, lithium batteries, temperature-dependent electrolytes, weak solvation structures

Received: November 17, 2022

Revised: January 23, 2023

Published online:

- [1] J. W. Yeh, S. K. Chen, S. J. Lin, J. Y. Gan, T. S. Chin, T. T. Shun, C. H. Tsau, S. Y. Chang, *Adv. Eng. Mater.* **2004**, *6*, 299.
- [2] B. Cantor, I. T. H. Chang, P. Knight, A. J. B. Vincent, *Mater. Sci. Eng., A* **2004**, *375–377*, 213.
- [3] E. P. George, D. Raabe, R. O. Ritchie, *Nat. Rev. Mater.* **2019**, *4*, 515.
- [4] C. M. Rost, E. Sacht, T. Borman, A. Moballeggh, E. C. Dickey, D. Hou, J. L. Jones, S. Curtarolo, J.-P. Maria, *Nat. Commun.* **2015**, *6*, 8485.
- [5] N. Dragoe, D. Bérardan, *Science* **2019**, *366*, 573.
- [6] A. Sarkar, Q. Wang, A. Schiele, M. R. Chellali, S. S. Bhattacharya, D. Wang, T. Brezesinski, H. Hahn, L. Velasco, B. Breitung, *Adv. Mater.* **2019**, *31*, 1806236.
- [7] Y. Sun, S. Dai, *Sci. Adv.* **2021**, *7*, eabg1600.
- [8] D. Bérardan, S. Franger, D. Dragoe, A. K. Meena, N. Dragoe, *Phys. Status Solidi RRL* **2016**, *10*, 328.
- [9] C. Zhao, F. Ding, Y. Lu, L. Chen, Y. S. Hu, *Angew. Chem., Int. Ed.* **2020**, *59*, 264.
- [10] K. Xu, *Chem. Rev.* **2014**, *114*, 11503.
- [11] B. Dunn, H. Kamath, J.-M. Tarascon, *Science* **2011**, *334*, 928.
- [12] K. Xu, *Chem. Rev.* **2004**, *104*, 4303.
- [13] Q. Wang, C. Zhao, S. Wang, J. Wang, M. Liu, S. Ganapathy, X. Bai, B. Li, M. Wagemaker, *J. Am. Chem. Soc.* **2022**, *144*, 21961.
- [14] D. Aurbach, E. Pollak, R. Elazari, G. Salitra, C. S. Kelley, J. Affinito, *J. Electrochem. Soc.* **2009**, *156*, A694.
- [15] Y. Liu, D. Lin, Y. Li, G. Chen, A. Pei, O. Nix, Y. Li, Y. Cui, *Nat. Commun.* **2018**, *9*, 3656.
- [16] Q. Shi, Y. Zhong, M. Wu, H. Wang, H. Wang, *Proc. Natl. Acad. Sci. USA* **2018**, *115*, 5676.
- [17] W. Zhang, Q. Wu, J. Huang, L. Fan, Z. Shen, Y. He, Q. Feng, G. Zhu, Y. Lu, *Adv. Mater.* **2020**, *32*, 2001740.
- [18] C. Yan, Y.-X. Yao, X. Chen, X.-B. Cheng, X.-Q. Zhang, J.-Q. Huang, Q. Zhang, *Angew. Chem., Int. Ed.* **2018**, *57*, 14055.
- [19] Y. Jie, X. Liu, Z. Lei, S. Wang, Y. Chen, F. Huang, R. Cao, G. Zhang, S. Jiao, *Angew. Chem., Int. Ed.* **2020**, *59*, 3505.
- [20] X. Wang, S. Wang, H. Wang, W. Tu, Y. Zhao, S. Li, Q. Liu, J. Wu, Y. Fu, C. Han, F. Kang, B. Li, *Adv. Mater.* **2021**, *33*, 2007945.
- [21] P. Arora, R. E. White, M. Doyle, *J. Electrochem. Soc.* **1998**, *145*, 3647.
- [22] H. Yang, X. Chen, N. Yao, N. Piao, Z. Wang, K. He, H.-M. Cheng, F. Li, *ACS Energy Lett.* **2021**, *6*, 1413.
- [23] S. C. Kim, X. Kong, R. A. Vilá, W. Huang, Y. Chen, D. T. Boyle, Z. Yu, H. Wang, Z. Bao, J. Qin, Y. Cui, *J. Am. Chem. Soc.* **2021**, *143*, 10301.
- [24] W. Zhang, H. Xia, Z. Zhu, Z. Lv, S. Cao, J. Wei, Y. Luo, Y. Xiao, L. Liu, X. Chen, *CCS Chem.* **2021**, *3*, 1245.
- [25] X. Dong, Y. Lin, P. Li, Y. Ma, J. Huang, D. Bin, Y. Wang, Y. Qi, Y. Xia, *Angew. Chem., Int. Ed.* **2019**, *58*, 5623.
- [26] S. Li, W. Zhang, Q. Wu, L. Fan, X. Wang, X. Wang, Z. Shen, Y. He, Y. Lu, *Angew. Chem., Int. Ed.* **2020**, *59*, 14935.
- [27] Y. Yamada, J. Wang, S. Ko, E. Watanabe, A. Yamada, *Nat. Energy* **2019**, *4*, 269.
- [28] Y. Rosenfeld, *Phys. Rev. A* **1977**, *15*, 2545.
- [29] J. C. Dyre, *J. Chem. Phys.* **2018**, *149*, 210901.
- [30] P. Argyrakis, A. Milchev, V. Pereyra, K. W. Kehr, *Phys. Rev. E* **1995**, *52*, 3623.
- [31] Q. Wang, Z. Yao, C. Zhao, T. Verhallen, D. P. Tabor, M. Liu, F. Ooms, F. Kang, A. Aspuru-Guzik, Y.-S. Hu, M. Wagemaker, B. Li, *Nat. Commun.* **2020**, *11*, 4188.
- [32] B. D. Adams, J. Zheng, X. Ren, W. Xu, J.-G. Zhang, *Adv. Energy Mater.* **2018**, *8*, 1702097.
- [33] D. Aurbach, Y. Gofer, J. Langzam, *J. Electrochem. Soc.* **1989**, *136*, 3198.
- [34] M. J. Zachman, Z. Tu, S. Choudhury, L. A. Archer, L. F. Kourkoutis, *Nature* **2018**, *560*, 345.
- [35] Z. Zhang, Y. Li, R. Xu, W. Zhou, Y. Li, S. T. Oyakhire, Y. Wu, J. Xu, H. Wang, Z. Yu, D. T. Boyle, W. Huang, Y. Ye, H. Chen, J. Wan, Z. Bao, W. Chiu, Y. Cui, *Science* **2022**, *375*, 66.
- [36] S. Chandrashekar, N. M. Trease, H. J. Chang, L.-S. Du, C. P. Grey, A. Jerschow, *Nat. Mater.* **2012**, *11*, 311.
- [37] R. Bhattacharyya, B. Key, H. Chen, A. S. Best, A. F. Hollenkamp, C. P. Grey, *Nat. Mater.* **2010**, *9*, 504.
- [38] D. Hubble, D. E. Brown, Y. Zhao, C. Fang, J. Lau, B. D. McCloskey, G. Liu, *Energy Environ. Sci.* **2022**, *15*, 550.
- [39] Y. Ugata, Y. Chen, S. Sasagawa, K. Ueno, M. Watanabe, H. Mita, J. Shimura, M. Nagamine, K. Dokko, *J. Phys. Chem. C* **2022**, *126*, 10024.
- [40] G. G. Eshetu, X. Judez, C. Li, M. Martinez-Ibañez, I. Gracia, O. Bondarchuk, J. Carrasco, L. M. Rodriguez-Martinez, H. Zhang, M. Armand, *J. Am. Chem. Soc.* **2018**, *140*, 9921.
- [41] C. Wang, Y. S. Meng, K. Xu, *J. Electrochem. Soc.* **2018**, *166*, A5184.